IEEE Access
Multidisciplinary ⋮ Rapid Review ⋮ Open Access Journal

Received November 14, 2019, accepted December 16, 2019, date of publication December 23, 2019,
date of current version January 6, 2020.

Digital Object Identifier 10.1109/ACCESS.2019.2961700

Underactuated Coupled Nonlinear Adaptive Control Synthesis Using U-Model for Multivariable Unmanned Marine Robotics

NUR AFANDE ALI HUSSAIN[1], SYED SAAD AZHAR ALI[1], MARK OVINIS[2], MOHD RIZAL ARSHAD[3], AND UBAID M. AL-SAGGAF[4]

[1]Centre for Intelligent Signal and Imaging Research (CISIR), Department of Electrical and Electronic Engineering, Universiti Teknologi PETRONAS, Seri Iskandar 32610, Malaysia
[2]Department of Mechanical Engineering, Universiti Teknologi PETRONAS, Seri Iskandar 32610, Malaysia
[3]School of Electrical and Electronic Engineering, Universiti Sains Malaysia Engineering Campus, Nibong Tebal 14300, Malaysia
[4]Center of Excellence in Intelligent Engineering Systems, King Abdulaziz University, Jeddah 21589, Saudi Arabia

Corresponding author: Syed Saad Azhar Ali (saad.azhar@utp.edu.my)

ABSTRACT This paper presents the control modelling and synthesis using a coupled multivariable under-actuated nonlinear adaptive U-model approach for an unmanned marine robotic platform. A nonlinear marine robotics model based on the dynamic equation using the Newtonian method and derivation with respect to the kinematics equations and rigid-body mass matrixes are explained. This nonlinear marine robotics model represents the underwater thruster dynamics, marine robotics dynamics and kinematics related to the earth-fixed frame. Coupled multivariable nonlinear adaptive control synthesis using a U-model approach for the Remotely Operated Vehicle (ROV) and Unmanned Surface Vessel (USV) represent an unmanned marine robotics application. A comparison is presented for the proposed nonlinear control approach between the U-model control approach with nonlinear Fuzzy Logic Control and Sliding Mode Control for the ROV and USV platforms. The results show minimum mean square error values and tracking performance between the plant or system model with the proposed method. Lastly, robustness and stability analysis for the proposed U-Model nonlinear control approach are presented by implementing an adaptive learning rate value.

INDEX TERMS Adaptive control, nonlinear, ROV, underactuated, unmanned marine robotics, USV.

I. INTRODUCTION

The robotics platform has become popular in many applications that involve land, sea and space. It can be fitted with various equipment, sensors and transducers for specific tasks. Unmanned marine robotics can be used efficiently to understand ocean characteristics and water environment issues and to protect the natural resources from these effects. Based on the current advancements in telecommunications technology, embedded controllers, open source systems and other related technology, robotic platforms can be deployed and controlled anywhere in the world, including harsh marine and water environments without human intervention. Unmanned marine robotics can be divided into two categories, namely unmanned surface vessels (USV) and unmanned underwater vehicles (UUV). UUV can be divided into two categories such as remotely operated using an umbilical cord or a remotely operated vehicle (ROV) and the second is without an umbilical cord or an autonomous underwater vehicle (AUV). USVs are operated on the surface of the water similar to a moving ship or vessel. However, a UUV is operated underwater. An ROV has an umbilical cord or a power and data cable extending from the surface to the vehicle. Thus, the vehicle can be controlled remotely from the surface while an AUV is operated autonomously. An ROV can perform with online data and for a longer duration underwater with heavy equipment due to the unlimited power supply from the surface with a limited coverage area while an AUV can cover a wide underwater area without any supervision and with a reduced operating crew. An AUV platform can manoeuvre freely underwater using underwater thrusters or by using a buoyancy engine mechanism that works by decreasing or increasing the buoyancy force. This functions intermittently much like an underwater glider for better coverage.

The associate editor coordinating the review of this manuscript and approving it for publication was Zheng Chen.

During the early development phase, these unmanned robotic platforms are made to achieve a specific operational task, but now such platforms can be used to perform multiple tasks and satisfy various objectives. With different designs and shapes, unmanned marine robotic platforms are highly nonlinear, underactuated with a limited control actuator, highly coupled in motion and vulnerable to external disturbances. The underactuated system needs to overcome the nonlinearity of the dynamics plus any disturbances and uncertainties arising from the marine environment [1]–[6]. The descriptive details of the unmanned marine robotic classes can be seen in Fig. 1.

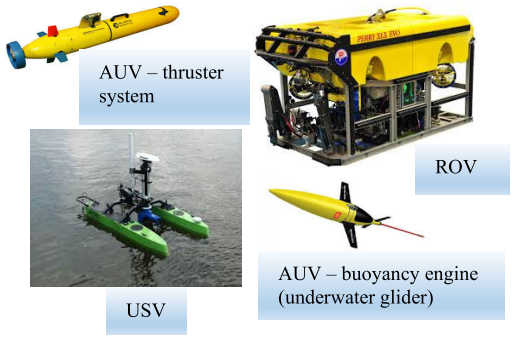

FIGURE 1. Unmanned marine robotic platforms [7]–[10].

Most of the platforms are multiple-input multiple output (MIMO) due to the installation of multiple sensors and transducers onboard. Unfortunately, there is no such precise approach for nonlinear control and modelling frameworks in the presence of external disturbances. In significant cases, the control framework outline strategies for nonlinear control systems vary from one framework to another. A few methodologies are described for nonlinear control framework plans in the literature which attempt to represent nonlinear control systems.

The underactuated trajectory control problem of an AUV in the presence of environmental disturbances was proposed by [11]. This scheme implemented the barrier Lyapunov function for control law combined with a backstepping algorithm, and a radial basis function neural network (RBFNN) with dynamic surface control for solving the effects of external disturbances. The proposed method was compared with the quadratic Lyapunov function and produced better tracking results via simulation. Another underactuated trajectory control approach for an AUV under perturbations was achieved using adaptive sliding mode control [12]. The sliding mode adaptive control was compared to the generalised super-twisting algorithm (GSTA) sliding mode via experiment using a Leonard ROV. The adaptive sliding mode method converged onto the desired input better than the GSTA approach with a reduced root-mean-square error value. Another control approach for the ROV platform used a double-loop sliding mode control for improvement of chatter reduction and to lower the root mean square error value [13]. Those authors introduced a novel switching term to replace the conventional switching term for sliding mode control. Several other works employed the sliding mode control approach for an AUV such as in [14], [15]. A recent sliding mode control approach for improved stability and convergence speed in the presence of chattering effect using time delay estimation and control is implemented in real-time for similar applications [16], [17]. An adaptive fuzzy sliding mode controller was proposed to estimate the nonlinearity of MIMO underwater vehicles in [18]. This method was the combination of two different nonlinear controllers aimed to counter the dynamics, chatter effect from the sliding mode control and from external disturbances. The fuzzy logic control approximates the coupled dynamics of the AUV. However, this method needs to be integrated with the sliding mode controller for stability analysis and the systematic control design method. The controller design was more complex and has a higher computational demand. The fuzzy logic control could reduce the chatter effect caused by the discontinuity of the sliding mode control system excited by unmodelled dynamics. In [19], a trajectory 3-D tracking control system was addressed for an AUV with a prescribed performance under model uncertainties and external disturbances. Control tracking with a specified performance converged to the desired values with minimal error. However, only specified performances are presented for torpedo-like MIMO vehicles and unicycle-like MIMO vehicles.

However, for USV applications the controller design can be challenging due to the need for rapid changing speed and manoeuvres. The nonlinearity effect will be severe during high speed manoeuvres thus the controller performance will be reduced or even fail. This is because the body of the USV platform is in direct contact with the water surface that influences the hydrodynamic flow. In [20] another combination of different controllers or a hybrid approach was employed for underactuated USV speed and heading control. A port-Controlled Hamiltonian controller and a back-stepping control method were combined for fast dynamic response and minimum controller energy usage. However, the USV model neglected drag and disturbance uncertainties. A new control law approach of trajectory tracking of the USV with disturbance parameters was proposed by [21]. The controller implemented dynamic surface control and active disturbance rejection control. The stability was proven through the Lyapunov function and the controller performance was compared via simulation with the sliding mode control. Another method of an underactuated and coupled system was by using an adaptive path following control for the USV. Adaptive neural networks (NN) including an active surface with minimal learning parameters was implemented to overcome parameter uncertainties and nonlinear disturbances [22]. RBFNN was embedded with the controller for rejection of uncertainties and nonlinear function approximation. These works demonstrated a smaller computational demand during the control synthesis process. However, this work naturally could not attend to every detail of the control design. Another USV control approach in [23] introduced an integral line of sight

for an extensive path following task. A modelling framework was established by considering the kinematic and dynamic disturbances to formulate a control law. Using a complex modelling approach, the control law was defined based on the control objectives and to sustain the stability conditions. A multi-loop adaptive control approach, with estimated disturbance rejection for similar applications, is presented and analysed by [24].

It is desirable to have a control structure that is capable of overcoming external disturbances without involving a complex mathematical and modelling approach. A reference-based model approach such an internal model control (IMC) structure can be implanted for a control strategy without any predefined precise mathematical modelling plus it includes a disturbance rejection capability. In [25], an IMC control structure was implemented for the rotors of a nonlinear MIMO vertical take-off and landing unmanned aerial vehicle (UAV). The relationship of the derivatives of the output and the changes in the tracking error were defined for the inverse implementation of the dynamic model. Then a flatness property was created for which all the system states and inputs could be determined from the outputs without any integration. The control system converged to the desired values with good system stability.

Other work was done by [26] using two degrees of freedom IMC-PID with logarithmic approximations for the load frequency controller of a power system. The inverse component made use of a low pass filter to reject any load disturbances. The control structure required another feedback controller to counteract the effects of befuddling or mismatching. The results showed good performance in terms of error analysis, settling time and disturbance rejection. Based on the literature, a variety of approaches are available when designing a nonlinear controller for an unmanned marine robotics platform, especially for the underactuated model and these approaches can be highly robust against external disturbances. It is difficult to design a controller that is suitable for all varieties of unmanned marine robotics due to the different operating requirements such as slow speed for the AUV platform and nominal to high speed for a USV in the presence of external disturbances.

The existing controller for unmanned marine robotic application mostly implemented decoupled technique for faster modelling and computation process. The approach is suitable for fully actuated system and some modification and assumption must be made for underactuated unmanned marine robotics platform. This paper implements a nonlinear coupled and multivariable adaptive control synthesis using the U-model for nonlinear unmanned marine robotic applications. Recently, U-model control technique has been implemented for SISO and MIMO in different process control engineering [27]–[29] and nonlinear dynamic plant [30]. Then implemented in robotic manipulator system by [31] and implemented for depth control of underwater glider platform [32]. Due to the nonlinearity of the platforms, the U-model control approach is further improved by applying a neural network algorithm for capturing nonlinearity in the system. This method also proven in term of improving the convergence speed. This control synthesis method uses only single-layer neural networks with an RBF activation function that has been implemented by [33]–[36]. This paper presents U-model based adaptive control approach for multivariable underactuated systems. The proposed approach is designed to be robust in rejecting external disturbance under payload variations for unmanned marine robotics applications using a simplified model and controller architecture.

This paper is organized as follows. Section II provides the nonlinear U-model modelling and control approach. Section III presents the convergence and robustness analysis of the proposed work. Section IV simulation parameters and controller comparison with Fuzzy Logic Control and Sliding Mode Control. Section V present the unmanned marine robotics modelling while section VI presents the result and discussions and conclusion of this work in section VII.

II. NONLINEAR U-MODEL MODELLING & CONTROL

A. NONLINEAR INTERNAL MODEL CONTROL APPROACH

An Internal Model Control (IMC) is selected as a nonlinear modelling control framework. Fig. 2 shows an IMC control structure. IMC approach is a popular choice in process control applications and effective with linear plants [25].

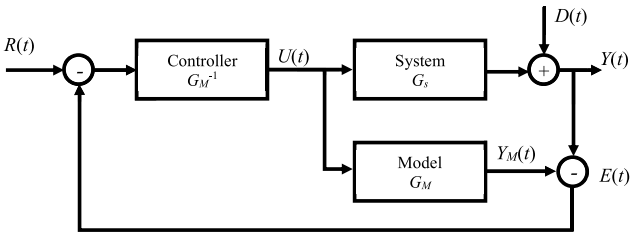

FIGURE 2. General IMC structure.

The IMC control structure consists of a reference input $R(t)$, a linear or nonlinear system Gs, a model of Gs or G_M, the controller as the inverse of G_M in the presence of unknown external disturbance $D(t)$ and output of the nonlinear system $Y(t)$. The output $Y(t)$ is compared with the model output $Y_M(t)$ to calculate the error $E(t)$. The closed loop system of the IMC control scheme can be expressed by [37]:

$$Y(t) = \frac{(R(t) - D(t))\, G_M{}^{-1} Gs}{1 + (Gs - G_M)\, G_M{}^{-1}} + D(t) \tag{1}$$

Rearranging Eq. (1), we get,

$$Y(t) = \frac{Gs Y_M{}^{-1} R(t) + (1 - Y_M{}^{-1} Y_M) D(t)}{1 + (Gs - Y_M) Y_M{}^{-1}} \tag{2}$$

Eq. (2) shows that according to IMC scheme, if the system can be truly modelled and the model can be inverted, it is possible reject the disturbances and output tracking is achieved. Therefore, the IMC tracking problem transforms to identifying a true model and its inverse. Recently, U-model has

been used for certain process control, robotics and other nonlinear SISO and MIMO applications. Therefore, this paper focuses on MIMO U-model based methodology for underwater marine applications.

B. COUPLED UNDERACTUATED MIMO NONLINEAR ADAPTIVE U-MODEL CONTROL SYNTHESIS APPROACH

The representation of a nonlinear equation using a Nonlinear AutoRegressive Moving Average with eXogenous input (NARMAX) is desirable due to the expansion of the nonlinear functions. It can be portrayed to a wide class of nonlinear frameworks [38]. NARMAX is a nonlinear function that consists of lagged output, input and prediction errors. The equation can be expressed as:

$$y(t) = f(y(t-1)\ldots y(\text{t-n})\, u(t-1) \ldots (\text{t-n}) + d(t-1)\ldots d(\text{t-n})), \quad (3)$$

The U-model can be obtained by expanding the NARMAX as in (3) as a polynomial of the control variable, $u(t-1)$ as follows:

$$y(t) = \sum_{j=0}^{N} \beta_j(t)\, u^j(t-1) + d(t) \quad (4)$$

where N is the degree of model input $u(t-1)$, $\beta_j(t)$ is a function of past inputs and outputs $u(t-1), \ldots, u(t-n)$, $y(t-1), \ldots, y(t-n)$ and errors $d(t-1), \ldots, d(t-n)$. β_j are matrices and updated online using the gradient descent algorithm. In this work, the normalised least mean square (nLMS) approach is used for updating the parameters. The SISO U-model can be extended for a n-input $\times r$-output multivariable system as a function of the control variable, $U(t-1)$ as:

$$Y_m(t) = G(U(t-1)) = \sum_{j=0}^{N} B_j U^j(t-1)$$
$$Y_m(t) = B(t)\, U(t-1) \quad (5)$$

$Y_m(t)$ is an $r \times 1$ output vector, and $U(t-1)$ is the $n \times 1$ control input vector. $B_j = [B_0, B_1, \ldots, B_N]$ are system parameters and function of past inputs and outputs. N is the degree of the multivariable polynomial $U^j(t-1)$ is the vector with j^{th} power of the i^{th} control inputs, $U_i(t-1)$ as,

$$U^j(t-1) = [U_1^j(t-1) U_2^j(t-1) \ldots U_n^j(t-1)]^T \quad (6)$$

A coupled MIMO nonlinear U-model control structure for n-inputs and r-outputs is shown in Fig. 3.
Thus, the formulation of the coupled underactuated n-input $\times$ r-output MIMO nonlinear U-model can be described as Eq. (7-11):

$$Y(t) = \left[Y_1(t), Y_{2,}(t), \ldots Y_r(t)\right]^T \quad (7)$$
$$U(t) = \left[U_1(t), U_{2,}(t), \ldots U_n(t)\right]^T \quad (8)$$
$$R(t) = \left[R_1(t), R_{2,}(t), \ldots R_r(t)\right]^T \quad (9)$$
$$Y_M(t) = \left[Y_{M1}(t), Y_{M2,}(t), \ldots Y_{Mr}(t)\right]^T \quad (10)$$

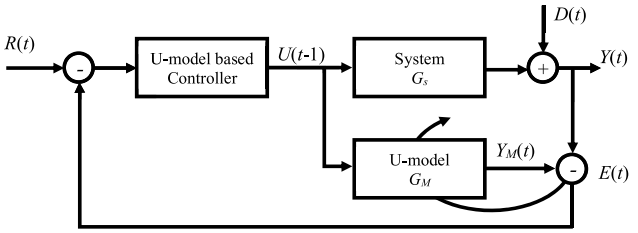

FIGURE 3. Coupled MIMO nonlinear U-model based IMC Structure.

$$E(t) = \left[E_1(t), E_{2,}(t), \ldots E_r(t)\right]^T \quad (11)$$

As an example of MIMO underactuated coupled U-model, a 2-input and 3-output U-model is demonstrated in Eq. (12).

$$\begin{pmatrix} Y_1 \\ Y_2 \\ Y_3 \end{pmatrix} = \begin{pmatrix} B_{011} & B_{111} & B_{211} & B_{311} & B_{021} & B_{121} & B_{221} & B_{321} \\ B_{012} & B_{112} & B_{212} & B_{312} & B_{022} & B_{122} & B_{222} & B_{322} \\ B_{013} & B_{113} & B_{213} & B_{313} & B_{023} & B_{123} & B_{223} & B_{323} \end{pmatrix} \times \begin{pmatrix} 1 \\ U_1 \\ U_1^2 \\ U_1^3 \\ 1 \\ U_2 \\ U_2^2 \\ U_2^3 \end{pmatrix} \quad (12)$$

All the inputs and outputs are coupled through the parameters, B_{jrn}. The subscripts j, r and n, represent the j^{th} power of control signal, r^{th} output, and n^{th} control input. Most of the marine robotic applications implement decoupling techniques to reduce difficulties during the modelling process. The shortcoming of this process is that it tends to reduce the efficiency of designing an excellent nonlinear controller. This novel coupled underactuated modelling approach can overcome the nonlinearity due to the dynamic interaction between the parameters and the disturbances.

The identification accuracy depends on the estimates of the system parameters, B_j. The parameters are recursively identified using nLMS algorithm. To enhance the identification, a nonlinear approximation using the Radial basis function (RBF) [39]–[41] approach is incorporated with U-model in order to capture the actual dynamics of the unknown nonlinearities in the ROV model. RBF has been reported to capture nonlinear dynamics with a single layer [36]. Integration of the U-model with an RBF nonlinear approximator will enhance the nonlinear modelling process such as in the previous work of the current authors [35]. The RBF is used to identify the only first element, B_{0ij}, in the U-model as in given by Eq. (13).

$$B_{0ij} = W(t)\, \phi(t) \quad (13)$$

The activation function can be expressed as in (14).

$$\phi(t) = \exp\left(-\frac{\|u(t-1) - c_i\|^2}{\beta^2}\right), \quad \text{for } i = 1, 2, \ldots, n \quad (14)$$

where n is the number of hidden layer neurons, c_i is the centre of the i^{th} hidden layer $(c_1, c_2, c_3..c_n)$node and β is the width of the activation function. Hence, the RBF weights $W(t)$ and the U-model parameters $B_j(t)$ $(j = 1, 2, N)$ are updated using nLMS as in Eq. (15) and Eq. (16).

$$W(t+1) = W(t) + \mu(t)E(t)\phi(t)^T \tag{15}$$

$$B_j(t+1) = B_j(t) + \mu(t)E(t)U^j(t-1)^T \tag{16}$$

The establishment of control law depends on development of the inverse of U-model. Since the U-model is a polynomial equation of the control signal $U(t-1)$, the control law can be synthesised using any polynomial root solving approach. The controller output $U(t-1)$ is obtained using the Newton-Raphson algorithm root solving method. Selecting the previous control signal as the initial value for the next time instant using Newton-Raphson is given by Eq. (17) [42]:

$$U_{i+1}(t-1) = U_i(t-1) - G'(U_i(t-1))^{-1} \times (G(U_i(t-1) - x(t)), \tag{17}$$

where i is the iteration index, $x(t)$ is the input to the controller or the feedback error, $U_i(t-1)$ is the output of the controller and G' is the Jacobian matrix with differential elements between all the outputs and the inputs [36]. $\mu(t)$ is the nLMS learning rate and has impact on convergence and robustness of the overall algorithm discussed in the next section.

III. CONVERGENCE AND ROBUSTNESS ANALYSIS

A. CONVERGENCE AND ROBUSTNESS ANALYSIS FOR AN UNDERACTUATED MIMO NONLINEAR ADAPTIVE U-MODEL

The IMC structure guarantees tracking in the presence of disturbance subject to the stability of overall feedback control loop. This requires the actual system to be stable at first place. For a stable system, overall closed loop stability is guaranteed if the model is a good stable approximation of the system and the inverse controller is also stable. Since, in U-model based IMC, the model is a polynomial in control variable of finite order and the inverse controller is the solution of the polynomial, both model and controller are stable. Therefore, the only condition for overall stability is to have the U-model convergence to the stable system [43]. The adaptive U-model implements recursive update procedure for weights update as in Eqs. (15) and (16) within a proper adaptation gain or learning rate value. This value should be in optimum range in order to converged to the desired value. It should neither too large and too small which would lead the system unstable and slowing the convergence process. Trial-and-error approach can be a common practice for learning rate value selection. Starting with smaller value of learning rate, that normally result in slower convergence speeds especially for multivariable systems with many weights mat effected amount of computation time. It is desirable to have an optimal learning rate with faster convergence speeds and keeping the algorithm stable. In this section, the selecting method of learning rate in order to guarantee robust tracking in the presence of noise and modelling uncertainties and to guarantee a faster convergence speed are discussed as in [44], [45]. Robustness and the stability of the control system can be defined as an ability to overcome external disturbances. A minor change of the external disturbance will lead to smaller changes in the estimation error. Robustness can be achieved if the ratio of an estimation error energy (E_E) to the disturbance energy (D_E) are upper bounded by positive constant as below:

$$\frac{E_E}{D_E} \leq 1 \tag{18}$$

Introducing a disturbance noise signal arising due to modelling error and noise $D(t)$. Based on Eq. (16), defining the optimal parameters of the actual system as $\grave{B}(t)$, the parameters can be estimated as $\tilde{B}(t)$. Based on the IMC approach the modelling error can be defined as:

$$E(t) = Y(t) - Y_M(t) \tag{19}$$

where the actual output is:

$$Y(t) = \grave{B}(t)U(t-1) + D(t) \tag{20}$$

And the model output is

$$Y_m(t) = \tilde{B}(t)U(t-1) \tag{21}$$

Therefore, Eq. (19) becomes

$$E(t) = \grave{B}(t)U(t-1) + D(t) - \tilde{B}(t)U(t-1) \tag{22}$$

$$E(t) = [\grave{B}(t) - \tilde{B}(t)]U(t-1) + D(t) \tag{23}$$

where $\grave{B}(t) - \tilde{B}(t)$ is the difference between the optimal parameter and its estimated values and can be represented as the parameter error, $\bar{B}(t)$. The modelling errors can be defined as the *a priori* error, $E_a(t)$ and *a posteriori* error, $E_p(t)$, before and after the update as:

$$E_a(t) = \bar{B}(t)U(t-1) \tag{24}$$

$$E_p(t) = \bar{B}(t+1)U(t-1) \tag{25}$$

These modelling errors can be rearranged as:

$$E_a(t) = (\grave{B}(t) - \tilde{B}(t))U(t-1) \tag{26}$$

$$E_a(t) = \grave{B}(t)U(t-1) - \tilde{B}(t)U(t-1) \tag{27}$$

$$E_a(t) = \grave{B}(t)U(t-1) - Y_M(t) \tag{28}$$

Combining the parameter update Eq. (16) and the *a posteriori* error in Eq. (25), we get,

$$E_p(t) = [\bar{B}(t) - \mu(t)E(t)U(t-1)^T]U(t-1) \tag{29}$$

$$E_p(t) = \bar{B}(t)U(t-1) - \mu(t)E(t)U(t-1)^T U(t-1) \tag{30}$$

$$E_p(t) = E_a(t) - \mu(t)E(t)||U(t-1)||^2 \tag{31}$$

The parameter error, $\bar{B}(t)$ also satisfies the update Eq. (16) as:

$$\bar{B}(t+1) = \bar{B}(t) - \mu(t)E(t)U(t-1)^T \tag{32}$$

In order to ensure the robustness of the system, the estimation error energy must be upper bounded by the disturbance energy or noise. The representation of the bounded energy can

be described as the estimation energy of the error-disturbance energy. It is desirable to obtain the estimation energy of the error upper bounded by disturbance energy in nature and in a practical system. Another parameter that needs to have an optimum value is the learning rate that guarantees the system to converge and robustness in tracking. The disturbance error can be defined as:

$$\tilde{D}(t) = E(t) - E_a(t) \tag{33}$$
$$E(t) = \tilde{D}(t) + E_a(t) \tag{34}$$

Now considering the error quantities, energy bound in Eq. (18), we evaluate energy for parameter error update Eq. (27) as:

$$\begin{aligned}&\left\|\bar{B}(t+1)\right\|^2 \\ &= \left(\bar{B}(t) - \mu(t) E(t) U(t-1)\right)^2 \\ &= \left\|\bar{B}(t)\right\|^2 - 2\mu(t)\bar{B}(t)\left(\tilde{D}(t) + E_a(t)\right) U(t-1) \\ &\quad + \mu(t)^2 \left\|U(t-1)\right\|^2 \left(\tilde{D}(t) + E_a(t)\right)^2\end{aligned} \tag{35}$$

Using the error value in Eq. (34), we get

$$\begin{aligned}\left\|\bar{B}(t+1)\right\|^2 = \left\|\bar{B}(t)\right\|^2 &- 2\mu(t) E_a(t)^2 - 2\mu(t) E_a(t)\tilde{D}(t) \\ &+ \mu(t)^2 \left\|U(t-1)\right\|^2 E_a(t)^2 \\ &+ 2\mu(t)^2 \left\|U(t-1)\right\|^2 E_a(t)\tilde{D}(t) \\ &+ \mu(t)^2 \left\|U(t-1)\right\|^2 \tilde{D}(t)^2\end{aligned} \tag{36}$$

Rearranging the terms:

$$\begin{aligned}&\left\|\bar{B}(t+1)\right\|^2 + 2\mu(t) E_a(t)^2 - \mu(t)^2 \left\|U(t-1)\right\|^2 E_a(t)^2 \\ &= \left\|\bar{B}(t)\right\|^2 - 2\mu(t) E_a(t)\tilde{D}(t) \\ &\quad + 2\mu(t)^2 \left\|U(t-1)\right\|^2 E_a(t)\tilde{D}(t) \\ &\quad + \mu(t)^2 \left\|U(t-1)\right\|^2 \tilde{D}(t)^2\end{aligned} \tag{37}$$

To simplify the equation, a new parameter $\acute{\eta}(t)$ is introduced as in Eq. (38):

$$\acute{\eta}(t) = \frac{1}{||U(t-1)||^2} \tag{38}$$

Therefore, Eq. (37) becomes,

$$\begin{aligned}&\left\|\bar{B}(t+1)\right\|^2 + 2\mu(t) E_a(t)^2 - \frac{\mu(t)^2}{(t)} E_a(t)^2 \\ &= \left\|\bar{B}(t+1)\right\|^2 - 2\mu(t) E_a(t)\tilde{D}(t) \\ &\quad + 2\frac{\mu(t)^2}{(t)} E_a(t)\tilde{D}(t) + \frac{\mu(t)^2}{(t)}\tilde{D}(t)^2\end{aligned} \tag{39}$$

If we set $\acute{\eta}(t) = \mu(t)$, we can simplify the Eq. (38) as,

$$\begin{aligned}&\left\|\bar{B}(t+1)\right\|^2 + 2\mu(t) E_a(t)^2 - \mu(t) E_a(t)^2 \\ &= \left\|\bar{B}(t)\right\|^2 - 2\mu(t) E_a(t)\tilde{D}(t) + 2\mu(t) E_a(t)\tilde{D}(t) \\ &\quad + \mu(t)\tilde{D}(t)^2\end{aligned}$$

or,

$$\left\|\bar{B}(t+1)\right\|^2 + \mu(t) E_a(t)^2 = \left\|\bar{B}(t)\right\|^2 + \mu(t)\tilde{D}(t)^2 \tag{40}$$

It can be concluded that the left-hand side of the equation represents the estimation energy of error while the right-hand side of the equation represents the disturbance energy for $\acute{\eta}(t) = \mu(t)$. Since, the Eq. (39) is a result of setting $\acute{\eta}(t) = \mu(t)$, we can three different conditions based on the value of learning rate, as:

$$\frac{\left\|\bar{B}(t+1)\right\|^2 + \mu(t) E_a(t)^2}{\left\|\bar{B}(t)\right\|^2 + \mu(t)\tilde{D}(t)^2} \begin{cases} = 1 & \text{for } 0 < \mu(t) < \acute{\eta}(t) \\ \geq 1 & \text{for } \mu(t) = \acute{\eta}(t) \\ \leq 1 & \text{for } \mu(t) > \acute{\eta}(t) \end{cases} \tag{41}$$

The first two conditions represent $\mu(t) \leq \acute{\eta}(t)$, thus computation from the signals $\{\bar{B}(t), \sqrt{\acute{\eta}(t)}E_p(t)\}$ to the signals $\{\bar{B}(t+1), \sqrt{\acute{\eta}(t)}E_a(t)\}$ is a lossless mapping. Regardless of what the noise energies impart and regardless of how far the parameter value varies from the ideal value the $\bar{B}(t)$ will be constantly less than or equal to the sum of the energies of the noise component, *i.e.*

$$\left\|\bar{B}(t+1)\right\|^2 + \mu(t) E_a(t)^2 \leq \left\|\bar{B}(t)\right\|^2 + \mu(t)\tilde{D}(t)^2$$

Hence, keeping $\mu(t) \leq \acute{\eta}(t)$, over the interval $0 < t < N$, ascertains that,

$$\left\|\bar{B}_N\right\|^2 + \sum_{t=0}^{N} \mu(t) E_a(t)^2 \leq \left\|\bar{B}_0\right\|^2 + \sum_{t=0}^{N} \mu(t)\tilde{D}(t)^2 \tag{42}$$

This ensures the tracking robustness of the U-Model under the influence of disturbance and noisy perturbations, resulting in an overall stability of the IMC loop. This can be extended to find a bound on the learning rate that guarantees Eq. (41).

To achieve a bound on the learning rate, consider Eq. (26), which can be represented in the feedback structure as an alternative form. The *a priori*error, $E_a(t)$, and the *a posteriori*error, $E_p(t)$ can be related by Equation (21) and expanded as follows:

$$E_p(t) = E_a(t) - \frac{\mu(t)}{\acute{\eta}(t)} E(t) \tag{43}$$
$$E_p(t)\acute{\eta}(t) = E_a(t)\acute{\eta}(t) - \mu(t) E(t) \tag{44}$$
$$\mu(t) E(t) = \acute{\eta}(t)\left(E_p(t) - E_a(t)\right) \tag{45}$$

Therefore, the nLMS recursive parameter error update in Eq. (27) could be written as:

$$\bar{B}(t+1) = \bar{B}(t) + \acute{\eta}(t) U(t-1)^T \left(E_a(t) - E_p(t)\right) \tag{46}$$

The energy of Eq. (45) can be calculated as:

$$\begin{aligned}&\left\|\bar{B}(t+1)\right\|^2 \\ &= \left\|\bar{B}(t)\right\|^2 \\ &\quad - 2\acute{\eta}(t)\bar{B}(t) U(t-1)\left(E_a(t) - E_p(t)\right) \\ &\quad + \acute{\eta}(t)^2 \left\|U(t-1)\right\|^2 \left(E_a(t) - E_p(t)\right)^2\end{aligned} \tag{47}$$

$$\begin{aligned}&\left\|\bar{B}(t+1)\right\|^2 \\ &= \left\|\bar{B}(t)\right\|^2 \\ &\quad - 2\acute{\eta}(t) E_a(t)\left(E_a(t) - E_p(t)\right)\end{aligned}$$

$$+\acute{\eta}(t)^2\frac{1}{(t)}E_a(t)^2-2\acute{\eta}(t)^2\frac{1}{(t)})E_a(t)E_p(t)+\frac{(t)^2}{(t)}E_p(t)^2 \quad (48)$$

$$\left\|\bar{B}\,(t+1)\right\|^2=\left\|\bar{B}\,(t)\right\|^2-2(t)E_a(t)^2+2\acute{\eta}(t)E_a(t)E_p(t)+(t)E_a\acute{\eta}(t)^2-2\acute{\eta}(t)E_a(t)E_p(t)+\acute{\eta}(t)E_p(t)^2 \quad (49)$$

$$\left\|\bar{B}\,(t+1)\right\|^2=\left\|\bar{B}\,(t)\right\|^2-\acute{\eta}(t)E_a(t)^2+\acute{\eta}(t)E_p(t)^2 \quad (50)$$

$$\left\|\bar{B}\,(t+1)\right\|^2+\acute{\eta}(t)E_a(t)^2=\left\|\bar{B}\,(t)\right\|^2+\acute{\eta}(t)E_p(t)^2 \quad (51)$$

$$\frac{\left\|\bar{B}\,(t+1)\right\|^2+\acute{\eta}(t)E_a(t)^2}{\left\|\bar{B}\,(t)\right\|^2+\acute{\eta}(t)E_p(t)^2}=1 \quad (52)$$

The expression in Eq. (51)) holds valid for all possible values of the learning rate. Eq. (51) implies that there is a lossless mapping $\bar{Si}$, from the signals $\{\bar{B}(t), \sqrt{\acute{\eta}(t)}E_p(t)\}$ to the signals $\{\tilde{B}(t+1), \sqrt{\acute{\eta}(t)}E_a(t)\}$ as in [43], [44].

In order find an optimum bound on the learning rate, the lossless mapping can be utilized along with small gain theorem. Considering the system and U-model outputs in Eqs. (20) and (21) and applying the mean-value theorem for at point ρ between $\grave{B}(t)U(t-1)$ and $\tilde{B}(t)U(t-1)$ during updating process gives:

$$\grave{B}(t)U(t-1)-\tilde{B}(t)U(t-1)=\dot{Y}_m(\rho)E_a(t) \quad (53)$$

where, $\dot{Y}_m(\rho)$ represents the derivative of the model output, $Y_m\,(t)$ at any point, ρ along the segment connecting $\grave{B}(t)U(t-1)$ and $\tilde{B}(t)U(t-1)$.

By combining Eq. (23) and Eq. (52),

$$E_p\,(t)=E_a\,(t)-\frac{\mu\,(t)}{(t)}\left((\grave{B}\,(t)-\tilde{B}\,(t))U\,(t-1)+D\,(t)\right) \quad (54)$$

$$E_p\,(t)=E_a\,(t)-\frac{\mu\,(t)}{(t)}\left(\dot{Y}_m(\rho)E_a(t)+D\,(t)\right) \quad (55)$$

$$E_p\,(t)=\left(1-\frac{\mu\,(t)}{(t)}\dot{Y}_m(\rho)\right)E_a\,(t)+D\,(t) \quad (56)$$

Rearranging Eq. (55) and multiplying by $\sqrt{\acute{\eta}(t)}$ to organise the feedback structure results in:

$$-\sqrt{\acute{\eta}(t)}E_p\,(t)=\frac{\mu\,(t)}{\sqrt{\acute{\eta}(t)}}D\,(t)-\left(1-\frac{\mu\,(t)}{\acute{\eta}\,(t)}\dot{Y}_m(\rho)\right)\times\sqrt{\acute{\eta}(t)}E_a\,(t) \quad (57)$$

Eq. (56) shows the mapping of the weighted disturbances, $\sqrt{\acute{\eta}(t)}D\,(t)$, to the resulting estimation error, $\sqrt{\acute{\eta}(t)}E_a\,(t)$. The relationship can be visualised in a feedback structure shown in Fig. 4 [43], [44].

Now that we have established the lossless mapping into a feedback structure, the stability of the feedback structure can be studied using small gain theorem. This allows us to utilize the adaptive learning rate established for the convergence and robustness of RBF neural networks in [36]. The weight update algorithm is mapped into a similar feedback structure and its stability and robustness is investigated using small gain theorem. Hence, a bound on the learning for U-model adaptation can be expressed as:

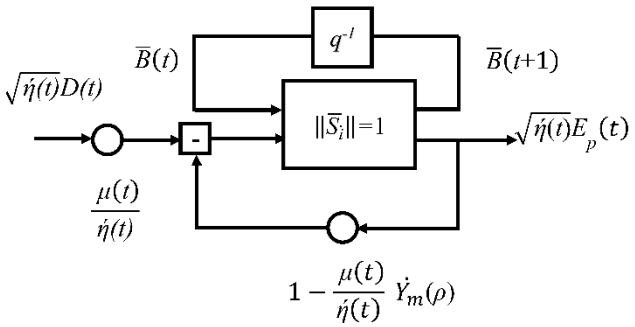

FIGURE 4. Lossless mapping with a feedforward and feedback structure.

$$0<\mu\,(t)\,\dot{Y}_m(t)<2\acute{\eta}(t)$$

Hence, the bound on the learning rate is,

$$\mu\,(t)<\frac{2}{\dot{Y}_m(t)\left\|U\,(t-1)\right\|^2} \quad (58)$$

The bound in Eq. (57) on the learning rate will ensure robustness and faster convergence. This will also guarantee that the overall U-model based IMC structure will remain stable.

IV. SIMULATION SETUP FOR RESULTS AND COMPARISONS

In this section, we present the unmanned marine robotics models used in the simulations along with the detail for benchmarking and comparison with the proposed controller. Fuzzy Logic Control (FLC) and Sliding Mode Control (SMC) approach was selected for benchmarking with the proposed method. Both methods are widely implemented in the UMV modelling and control application.

A. UNMANNED MARINE ROBOTICS MODELLING

1) NONLINEAR ROV MODEL

The standard notation of the Society of Naval Architects & Marine Engineers (SNAME) used for marine vehicles is shown in Table 1.

Using the Newtonian approach, the motion of a rigid body with respect to the body-fixed reference at the origin in Fig.5 is given by the following set of equations [46]:

$$M_{mass}[\dot{v_1}+v_2\times v_1+\dot{v_2}\times r_G+v_2\times(v_2\times r_G)]=\tau_1 \quad (59)$$

$$I\dot{v_2}+v_2\times(Iv_2)+M_{mass}\times r_G\times(v_1+\dot{v_2}\times v_1)=\tau_2 \quad (60)$$

where $r_G=[x_G\ y_G\ z_G]^T$ is the location of the centre of gravity, $\tau_1\in\check{R}^3$ and $\tau_2\in\check{R}^3$ are the external force and moment vector; $v_1=[u\ v\ w]^T\in\check{R}^3$ is the linear velocity

TABLE 1. Notation and variables for marine vehicles [46], [47].

DoF	Motion Description	Position and Orientation	Linear and Angular Velocity
1	Motion in the x-direction (surge)	x	u
2	Motion in the y-direction (sway)	y	v
3	Motion in the z-direction (heave)	z	w
4	Rotation about the x-axis (roll)	φ	p
5	Rotation about the y-axis (pitch)	θ	q
6	Rotation about the z-axis (yaw)	ψ	r

vector and $v_1 = [p\ q\ r]^T$ is the angular velocity vector. $M_{mass} \in \check{R}^{3x3}$ is the UUV mass matrix:

$$M_{mass} = \begin{bmatrix} m & 0 & 0 \\ 0 & m & 0 \\ 0 & 0 & m \end{bmatrix} = mI_{3\times 3} \tag{61}$$

$I_{3\times 3}$ is the identity matrix and $I \in \check{R}^{3\times 3}$. The rigid body equation consisting of inertia forces and the coriolis and centrifugal forces in matrix form can be expressed as:

$$M_{RB}\dot{v} + C_{RB}(v) = \tau \tag{62}$$

where $M_{RB} \in \check{\mathrm{R}}^{6\times 6}$ is the mass-inertia matrix, $C_{RB}(v)$ is the coriolis and centrifugal matrix, $\tau = [\tau_1\ \tau_2]^T \in \check{\mathrm{R}}^{6\times 6}$ is a vector of external forces and moments and $v = [v_1\ v_2]^T \in \check{\mathrm{R}}^{6\times 6}$ is the linear and angular velocity vector. The open loop nonlinear UUV dynamic equation can be expressed by:

$$M\dot{v} + C(v)v + D(v)v + G_f(\eta_2) = \tau = \tau_A + \tau_H \tag{63}$$

where $M_V = M_{RB} + M_A$, $C_V = C_{RB} + C_A$, $D(v)$ is the damping matrix due to the surrounding fluid and $G_f(\eta_2)$ is the gravitational and buoyancy matrix.

2) NONLINEAR USV MODEL

The USV nonlinear model is derived from similar principles as the nonlinear UUV except for the propulsion forces and moment equations. A USV is exposed to the wind, waves and current disturbances. The dynamic equation can be expressed by:

$$M\dot{v} + C(v)v + D(v)v + G_f(\eta_2) = w + \tau + g_o \tag{64}$$

where w is related to the wave disturbance, τ represents propulsion forces and moment, and g_o the restoring forces related to the ballast system. A detailed explanation of the modelling derivation of a USV is discussed in [47].

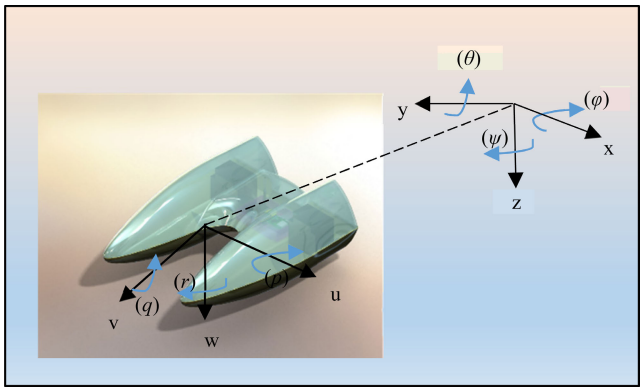

FIGURE 5. USV motion dynamics.

Fig. 5 shows the USV body-fixed reference at the origin that can be implemented in the UUV platform.

B. FUZZY LOGIC CONTROL SYNTHESIS APPROACH

The FLC design has three main components for the controller design, namely fuzzification, inference rules and defuzzification operations. Fuzzification involves defining the controlled inputs, normal system error, e and change of error, $\dot{e}$ ranging from 0 to 1. Next, the inference rules will define the membership functions involving activation functions, such as triangular and trapezoidal with linguistic variables defined as: Negative Big (NB), Negative Medium (NM), Negative Small (NS), Zero (Z), Positive Small (PS), Positive Medium (PM) and Positive Big (PB). Then, these linguistic values are transformed to a numerical value of the control variable as the output of the FLC control synthesis.

C. SLIDING MODE CONTROL SYNTHESIS APPROACH

The SMC introduces a sliding surface in terms of error by defining, $e = y - y_d$ and the surface error by $s = \dot{e} + \gamma e$ where γ is the bandwidth $(\gamma > 0)$. The Lyapunov function can be represented as:

$$V(s(t)) = \frac{1}{2}s^T Ms \tag{65}$$

Time derivative yields:

$$V(s(t)) = \frac{1}{2}s^T M\dot{s} \tag{66}$$

The control law can be defined as:

$$\bar{u} = u_{eq} + u_{sw} \tag{67}$$

where u_{eq} is related to the nonlinear dynamics and keeps the state of the system on the sliding surface, while u_{sw} is the switching control to force the system to slide on the sliding surface. Depending on the reaching law for sliding mode control applications, it will ensure the system will reach equilibrium. For example, the constant reaching law is as follows:

$$\dot{s} = -Fsgn(s) \tag{68}$$

where F is the tuning parameter and $sgn(s)$ is a function defined by:

$$sgn(s) = \begin{cases} 1, & s > 0 \\ 0, & s = 0 \\ -1, & s < 0 \end{cases} \tag{69}$$

The tracking and stability are achieved by $\dot{V} \leq 0$ thus $V \leq 0$ and therefore s is bounded. The application of Barbalat's lemma must comply $s \to 0$ and thus $e \to 0$ as $t \to \infty$. The shortcoming of this method is excessive discontinuous switching across $s = 0$ or chattering. However, a boundary layer around the s surface with thickness $\forall > 0$ can be implemented to reduce the chattering effect. While the platform dynamics remain inside this boundary layer then no switching is made. When the platform dynamics are outside the boundary layer then the switching is carried out by:

$$sat\left(\frac{s}{\forall}\right) = \begin{cases} sgn\left(\frac{s}{\forall}\right), & \text{for } \left|\left(\frac{s}{\forall}\right)\right| \geq 1 \\ \left(\frac{s}{\forall}\right), & \text{for } \left|\left(\frac{s}{\forall}\right)\right| < 1 \end{cases} \tag{70}$$

D. SIMULATION PARAMETERS

Coupled MIMO nonlinear, fuzzy logic and sliding mode adaptive modelling and control effort synthesis is carried out using the UUV and USV platforms to analyse the control performance. Simulation were performed using MATLAB^{TM} Simulink.

The UUV is based on a ROV platform consisting of four thrusters. Thruster 1 and 2 will control the x-axis (surge and sway) and the y-axis dynamics while thruster 3 and 4 are for the z-axis or heave as in Fig. 1. The matrices of the ROV platform are implemented based on the development presented in [46]. The ROV parameter matrices are given in Table 2.

Simulation of the control system for the USV platform is based on one thruster and one rudder system. The yaw angle (rudder) and surge force (underwater thruster) are the control inputs [48]. The yaw angle can be represented as the rudder position and the surge forces as the underwater thruster response model. They are coupled based on Equation (18). The mathematical model for a USV moving in a horizontal plane can be described as [22]:

$$\dot{x} = u\cos(\psi) - v\sin(\psi) \tag{71}$$

$$\dot{y} = u\sin(\psi) - \mathrm{v}\cos(\psi) \tag{72}$$

$$\dot{\psi} = r \tag{73}$$

$$\dot{u} = \frac{m_{22}}{m_{11}}vr - f_u(u) + \frac{1}{m_{11}}\tau_u + D_u \tag{74}$$

$$\dot{v} = -\frac{m_{11}}{m_{22}}ur - f_v(v) + D_v \tag{75}$$

$$\dot{r} = \frac{(m_{11} - m_{22})}{m_{33}}uv - f_r(r) + \frac{1}{m_{33}}\tau_r + D_r \tag{76}$$

where x, y and ψ are the surge, sway and yaw angle as in Table 1. Parameter τ_u and τ_r represent the control inputs related with surge forces and yaw moment while D_u, D_v and D_r are the external disturbances. Parameters f_u, f_v and f_r are the high order dynamic effect of the nonlinear functions. The Nomoto model can be implemented to represent the heading control for a single actuation thruster system. The Nomoto model [47] is obtained by eliminating the sway velocity v from the Davidson and Schiff model [49] into a second-order approximation:

$$\frac{\mathrm{r}}{\delta}(s) = \frac{\mathrm{K}(1+T_3 s)}{(1+T_1 s)(1+T_2 s)} \tag{77}$$

While the first order approximation is obtained by letting $T = T_1 + T_2 - T_3$, which yields:

$$\frac{\mathrm{r}}{\delta}(s) = \frac{K}{s(1+Ts)} \tag{78}$$

The linear approximation can be achieved by setting the desired yaw angle $\dot{\psi}_\mathrm{d} = 0$, $\sin(\psi) \approx 0$, $\cos(\psi) \approx 1$ and $\mathrm{u} \gg \mathrm{v}$ based on [48] yields:

$$x = \frac{u}{s} \tag{79}$$

$$y = \frac{Ku}{s^2(1+Ts)}\delta \tag{80}$$

An open loop underwater thruster model was developed by [50] and is implemented in the simulation process. The open loop transfer function of the underwater thruster system can be expressed by:

$$\mathrm{G}(s) = \frac{-28.77s + 16.28}{s^2 + 45.09s + 16.33} \tag{81}$$

Hence the reference input for the underwater thruster system is the reference speed u of the USV platform while the yaw angle ψ is the reference input for the first input.

TABLE 2. ROV parameter values.

Parameter	Matrix value
$M_{RB(6\times6)}$	$\begin{pmatrix} 115 & 0 & 0 & 0 & 0 & 0 \\ 0 & 115 & 0 & 0 & 0 & 0 \\ 0 & 0 & 115 & 0 & 0 & 0 \\ 0 & 0 & 0 & 6.1 & -1.6e-4 & -0.185 \\ 0 & 0 & 0 & -1.6e-4 & 5.98 & 6e-4 \\ 0 & 0 & 0 & -0.185 & 6e-4 & 9.59 \end{pmatrix}$
$T_{(6\times4)\ \text{thrusters}}$	$\begin{pmatrix} 1 & 1 & 0 & 0 \\ 0 & 0 & 0.7071 & -0.7071 \\ 0 & 0 & 0.7071 & 0.7071 \\ 0 & 0 & -0.293 & 0.293 \\ -0.016 & -0.016 & -0.012 & -0.012 \\ 0.31 & -0.31 & 0.012 & -0.012 \end{pmatrix}$
$D_{linear(6\times6)}$	$\begin{pmatrix} -26.114 & 0 & 0 & 0 & 0 & 0 \\ 0 & -29.996 & 0 & 0 & 0 & 0 \\ 0 & 0 & -59.044 & 0 & 0 & 0 \\ 0 & 0 & 0 & -11.75 & 0 & 0 \\ 0 & 0 & 0 & 0 & -15 & 0 \\ 0 & 0 & 0 & 0 & 0 & -29.522 \end{pmatrix}$
$D_{quadratic(6\times6)}$	$\begin{pmatrix} -145.76 & 0 & 0 & 0 & 0 & 0 \\ 0 & -170.52 & 0 & 0 & 0 & 0 \\ 0 & 0 & -351.98 & 0 & 0 & 0 \\ 0 & 0 & 0 & -65.59 & 0 & 0 \\ 0 & 0 & 0 & 0 & -85.26 & 0 \\ 0 & 0 & 0 & 0 & 0 & -10.63 \end{pmatrix}$
$M_{mass(3\times3)}$	$\begin{pmatrix} 115 & 0 & 0 \\ 0 & 115 & 0 \\ 0 & 0 & 115 \end{pmatrix}$
B=W	$1.1282\text{x}10^3$ N

1) SLIDING MODE CONTROL

In order to satisfy reaching the conditions of sliding mode control it is required that $s\dot{s} \leq 0$. The sliding mode controller output and parameters for the ROV and USV platforms are expressed in Table 3 and Table 4.

TABLE 3. Sliding Moe Control Parameter for The ROV.

ROV	$R_1(t)$	$R_2(t)$	$R_3(t)$
Controller output equation	$u(t)=(K_1\times s)/10$	$u(t)=(K_1\times s)/10$	$u(t)=(K_2\times s - s^2)/6$
Tuning parameter	$K_1 = 10$	$K_1 = 7$	$K_2 = 6$
Boundary thickness, ∀	0.1	0.1	0.1

TABLE 4. Sliding mode control parameter for The USV.

USV	$R_1(t)$	$R_2(t)$
Controller output equation	$u(t)=(K_1\times s)/10$	$u(t)=(K_2\times s - s^2)/6$
Tuning parameter	K_1=4	K_2=3
Boundary thickness, ∀	0.7	0.7

2) FUZZY LOGIC CONTROL

The FLC inference operation was implemented using 49 rules (or If-Then) statements. The implication-aggregation compositional rule of inference and the weighted average method were used in the deffuzzier process based on the Sugeno inference method. The rule table has the same output membership in a diagonal direction or Toeplitz structure, as shown in Table 5 and was implemented for the ROV and USV platforms.

TABLE 5. Controlled Inputs *e* & $\dot{e}$ for The FLC control synthesis.

Rule table with Toeplitz structure for Sugeno							
e \ $\dot{e}$	PL	PM	PS	Z	NS	NM	NL
NL	0	-0.25	-0.5	-0.75	-0.75	-0.75	-0.75
NM	0.25	0	-0.25	-0.5	-0.75	-0.75	-0.75
NS	0.5	0.25	0	-0.25	-0.5	-0.75	-0.75
Z	0.25	0.5	0.25	0	-0.25	-0.5	-0.75
PS	0.75	0.25	0.5	0.25	0	-0.25	-0.5
PM	0.75	0.75	0.25	0.5	0.25	0	-0.25
PL	0.75	0.75	0.75	0.25	0.5	0.25	0

3) COUPLED UNDERACTUATED MIMO U-MODEL

The coupled MIMO U-Model control synthesis for both platforms was carried out as shown in Figure 4. The reference inputs for the ROV platform are the thruster allocation for the x-axis, y-axis and z-axis underwater movements. $R_1(t)$ as the x-axis, $R_2(t) - y$-axis and $R_3(t)$ for z-axis. The simulation executes the 3D underwater manoeuvring with pre-defined input waypoint co-ordinates from (0, 0, 0), (5,5,1) and (10,10,2). For the USV platform, the simulation executes 2D surface movement by setting the reference input 1 - $R_1(t)$, ψ (yaw angle) and continuously changing course every 30 seconds (5°, 10°, 15°, 20°, 25°, 30°, 25° and 20°) while changing the surge speed u from 0.2 m/s, 0.4 m/s and 0.8 m/s for reference input 2 - $R_2(t)$. The sway speed v is assumed at 0.01 m/s as an external dynamic disturbance. These changing dynamics will influence the performance and stability of the control system to ensure a good tracking capability. The same control synthesis is implemented for the FLC and SMC for comparison with the coupled underactuated MIMO U-Model. The 3rd order system of the MIMO U-model with 5 neurons for the RBF neural networks with centres spaced at [0, 2.5, 5, 7.5, 10] radians for the ROV platform and [0, 0.5, 1, 1.5, 2] for the USV platform. The initial values for these neurons are equal parameter in Equation (16) is equal to 0.1 [0.1 0.1 0.1] and the learning rate value is equal to 0.3 for both the ROV and USV platforms.

V. RESULT AND DISCUSSIONS

A. ROV PLATFORM SIMULATION RESULTS

Based on the parameters above, a comparison between the U-Model, FLC and SMC control approach was carried out simultaneously using the MATLAB Simulink platform for the ROV and the results can be seen in Fig. 6 and Fig. 7. The comparison is made in terms of tracking the reference input, and the Mean Square Error (MSE) to evaluate the performance of the control synthesis. Fig. 6 (a-c) show that all the outputs converged to the desired reference inputs.

In x-direction and y-direction, the coupled U-model converged with better performance. In z-direction coupled SMC approach converged with better performance. This is because SMC used different control parameters for x, y, and z directions compared with U-Model and FLC approach. We observed a faster response, efficient convergence and smaller MSE using the proposed methodology. However, a slightly higher overshoot was observed with the proposed approach on some occasions. The overshoot may be reduced at the cost of slower response and higher MSE. In z-direction the vehicle needs to overcome the buoyancy force in upward direction thus effecting the control performances. However, U-Model and FLC approach can be further improved by tuning the control parameter to overcome the buoyancy force in z-direction. The detail comparison of these controller performances is present in the MSE analysis in x, y, and z directions in Fig. 6 (d-f). Coupled U-Model approach converged to smaller value in $x$and y directions while SMC scheme converged to smaller value in z-direction.

Fig. 7 shows the underwater 3D ROV movement based on the x, y, and z – directions reference values in all the controller approach.

Table 6 shows all the final steady state square error values according to the different time frames for the x, y, and z underwater manoeuvring directions with the coupled U-Model controller exhibiting the lowest error results except in z-direction due to higher damping cause by buoyancy force effect. This can be overcome by changing the learning rate value into appropriate value to overcome this effect.

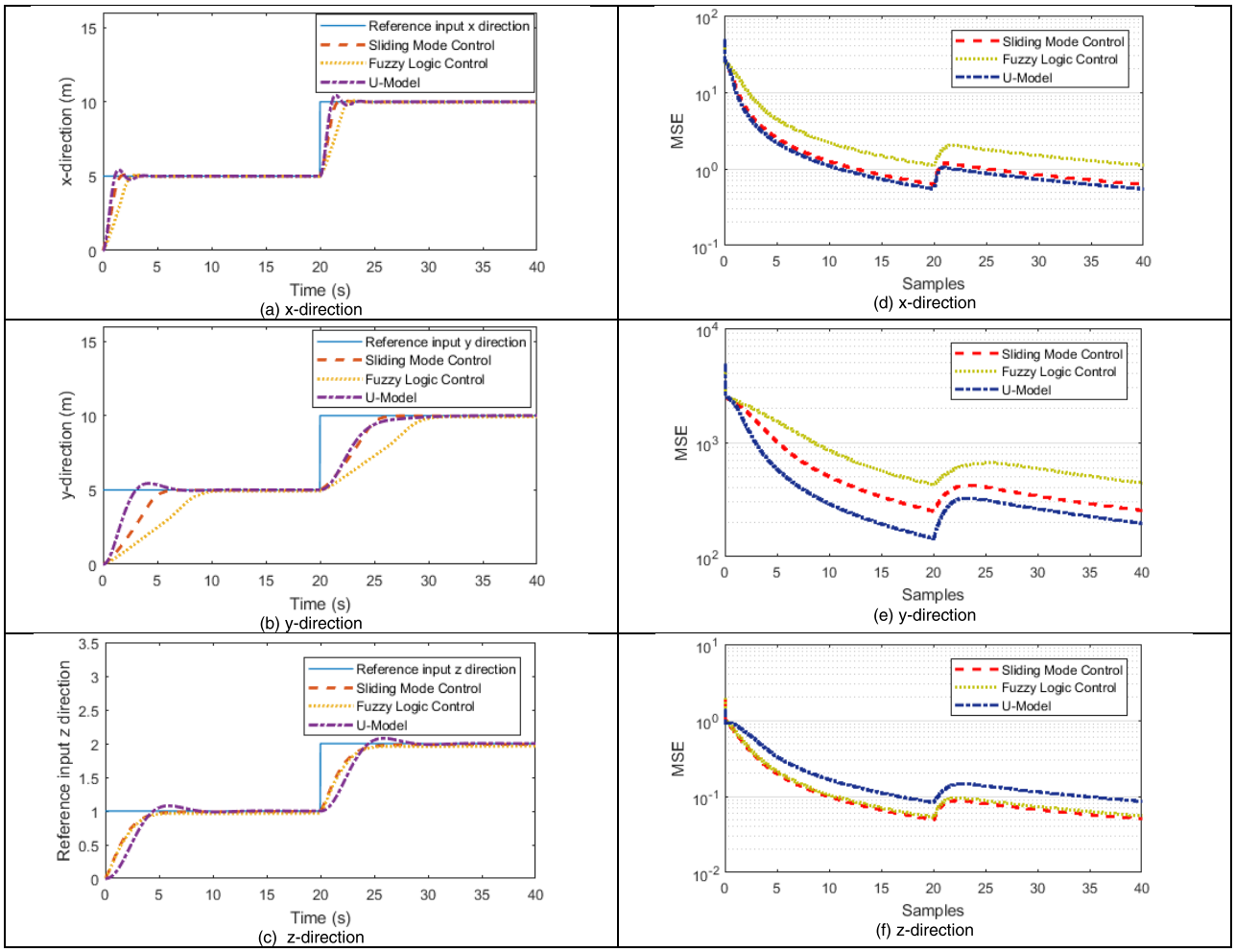

FIGURE 6. Comparison of control tracking and MSE analysis for the ROV platform.

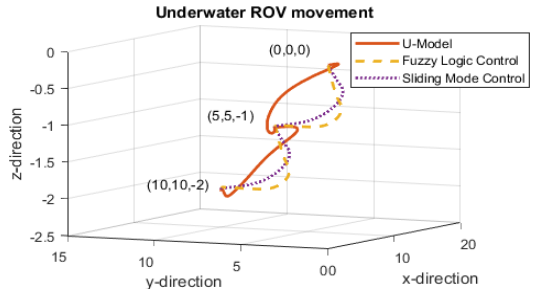

FIGURE 7. ROV Underwater trajectory comparison of controllers in *x-y-z* plane.

B. USV PLATFORM SIMULATION RESULTS

A comparison between the U-Model, FLC and SMC control approaches was carried out simultaneously using the MATLAB Simulink platform for the USV platform. The results are presented in Fig. 8.

According to the simulation results, all the control schemes converged to the desired reference input. The reference input was arranged to change its rudder angle every 30 seconds of manoeuvring. All the control approaches converged to the desired value with different control effort performances. The performances could be differentiated by the tracking capability by controller effort with respect to the reference input. The coupled U-Model controller had the lowest final MSE value. The number of samples and the sampling rate for the MSE computation were 24,000 and 100 Hz, respectively. It can be seen in Fig. 8(a) and Fig. 8(c) that the U-Model converges

TABLE 6. Convergence of mean square error values for each controller on The ROV platform.

Time frame and ROV direction	U-Model	FLC	SMC
(0 – 20) sec and x-direction	**0.55**	1.12	0.63
(0 – 20) sec and y-direction	**1.47**	4.33	2.55
(0 – 20) sec and z-direction	**0.051**	0.055	0.085
(20 – 40) sec and x-direction	**0.55**	1.13	0.63
(20 – 40) sec and y-direction	**1.98**	4.47	2.57
(20 – 40) sec and z-direction	0.087	0.056	**0.051**

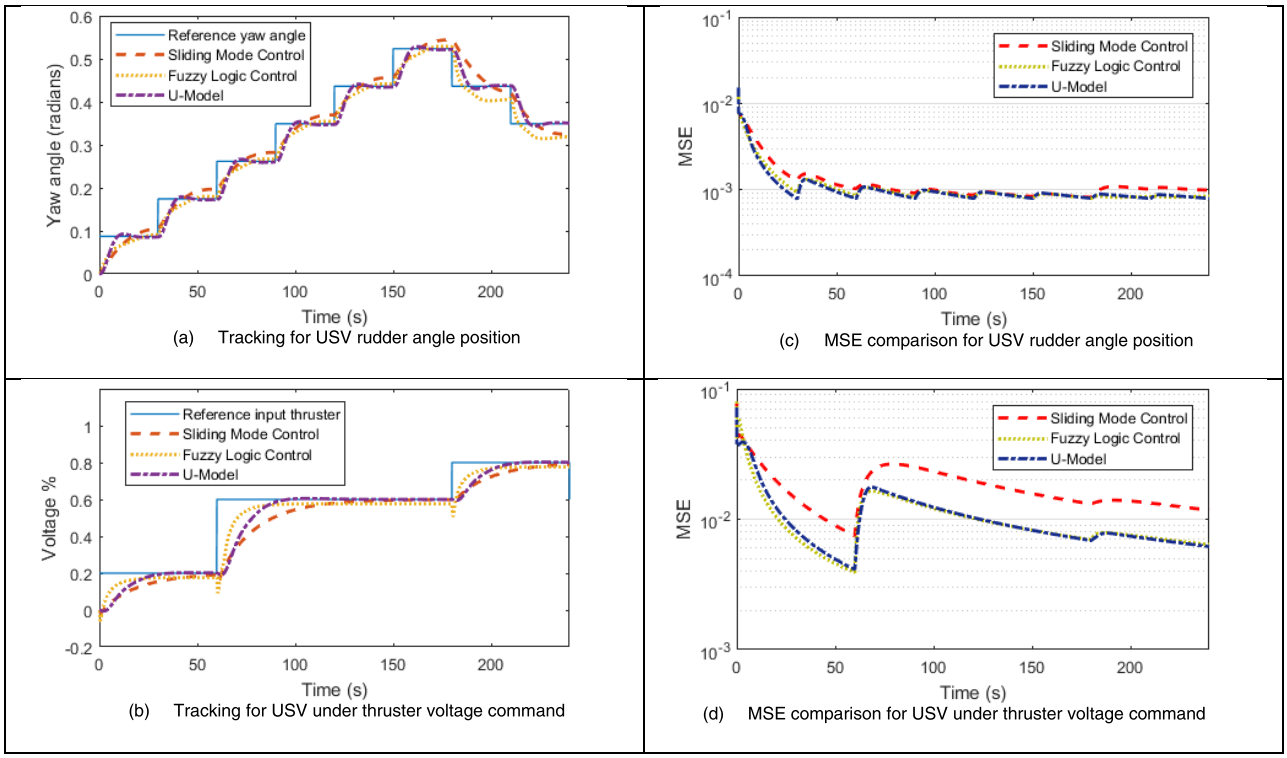

FIGURE 8. Comparison of control tracking and MSE analysis for the USV platform.

TABLE 7. Convergence of mean square error values for each controller in each rudder deflection the USV platform.

Time frame	U-Model	FLC	SMC
0 to 30 sec	**7.82 x 10^{-4}**	9.29 x 10^{-4}	1.30 x 10^{-3}
30 to 60 sec	**7.99 x 10^{-4}**	8.60 x 10^{-4}	1.00 x 10^{-3}
60 to 90 sec	**7.91 x 10^{-4}**	8.19 x 10^{-4}	9.12 x 10^{-4}
90 to 120 sec	**8.06 x 10^{-4}**	8.20 x 10^{-4}	8.71 x 10^{-4}
120 to 150 sec	**7.95 x 10^{-4}**	8.00 x 10^{-4}	8.35 x 10^{-4}
150 to 180 sec	7.93 x 10^{-4}	**7.92 x 10^{-4}**	8.14 x 10^{-4}
180 to 210 sec	8.66 x 10^{-4}	**8.24 x 10^{-4}**	1.10 x 10^{-3}
210 to 240 sec	**7.89 x 10^{-4}**	8.36 x 10^{-4}	9.88 x 10^{-4}

faster and has a smaller final value of the mean square error in the first 150 seconds of simulation compared to the FLC and the SMC except during 150 seconds to 210 seconds time frame. However, U-Model has the final minimum MSE value and can be summarised as given in Table 7 below.

Based on Table 7, the U-Model control synthesis has the minimum convergence square error values for all the different yaw angles during rudder deflection compared to the FLC and SMC approaches. The coupled underactuated U-Model converged faster for each rudder deflection time frame, thus giving the best performance in terms of tracking and final convergence values. The following results (Fig. 8(b) and Fig. 8(d)) will explain the second reference input – surge speed u that changed from 0.2 m/s, 0.4 m/s and 0.8 m/s during the simulation while Fig. 9 shows the reference trajectory

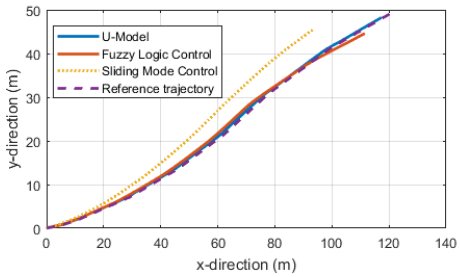

FIGURE 9. Trajectory comparison with different controller approaches for the USV platform in the *x-y* plane.

for the USV platform. U-model follows the actual position closely compare with FLC and SMC approaches. The same performance of the controllers was observed. FLC had a slightly better MSE value and faster convergence time. However, it had more significant square error values compared to the U-Model and SMC for each change in surge speed.

It was observed that for each change in surge speed, an overshoot occurred for the FLC approach. Tuning can be undertaken for all 49 rule-based statements. However, it is a time-consuming process. From Table 8, the U-Model exhibited the lowest square error values compared to the FLC and SMC approaches for all voltage input time frames.

From Table 8, the U-Model control synthesis had a minimum of convergence mean square error values during the speed changes of the UMV platform. The FLC converged with higher speed and better MSE values. However, overshoot occurred during these transition periods. The coupled

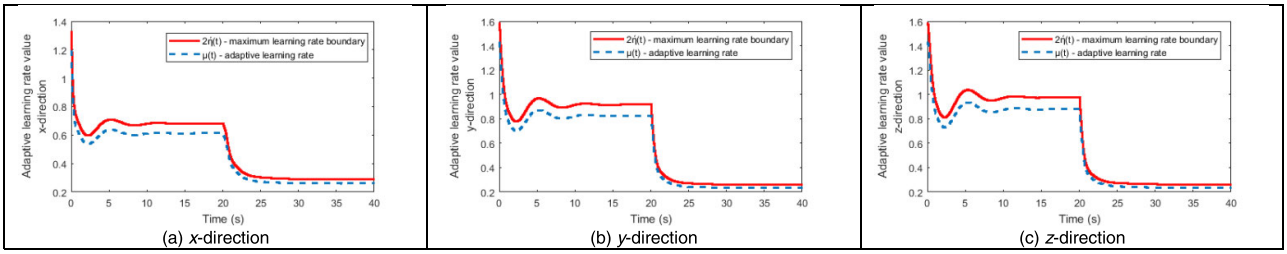

FIGURE 10. Adaptive learning rate variation for the ROV platform in x, y, and z-directions.

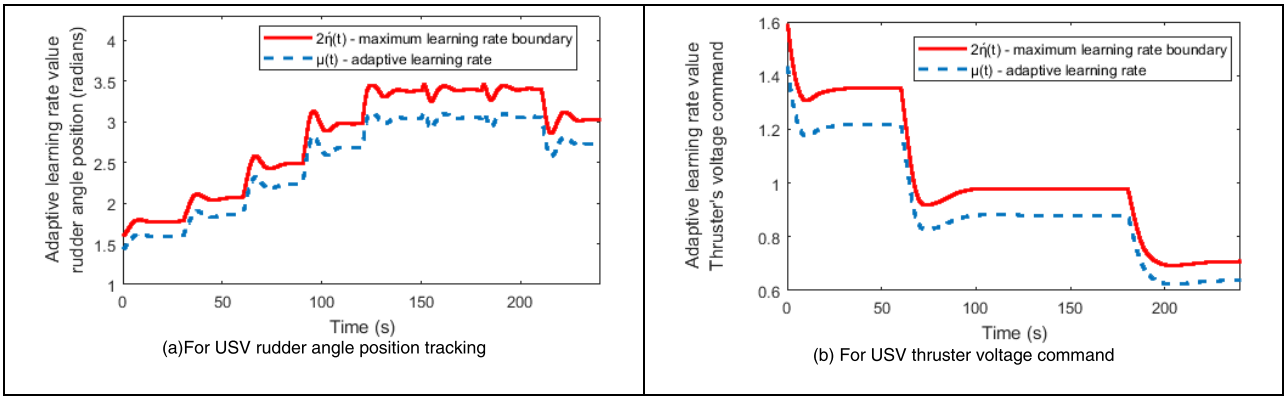

FIGURE 11. Adaptive learning rate variation for the USV platform.

TABLE 8. Convergence of mean square error values for each controller for each surge speed on The USV platform.

Time frame	U-Model	FLC	SMC
0 to 60 sec	4.10 x 10^{-3}	**3.90 x 10^{-3}**	7.50 x 10^{-3}
60 to 180 sec	**6.90 x 10^{-3}**	7.00 x 10^{-3}	1.31 x 10^{-2}
180 to 240 sec	**6.20 x 10^{-3}**	6.40 x 10^{-3}	1.17 x 10^{-2}

U-Model approach implemented the same initial learning rate, parameters and weight values for both the ROV and USV platforms without any tuning. Both learning rate values were fixed at 0.3 for the ROV and USV platforms.

C. RESULTS FOR CONVERGENCE AND ROBOUSTNESS ANALYSIS

The coupled U-Model approach can be further improved by the selection of a proper learning rate for better controller tracking, stability, and robustness. Using the same approach as the coupled U-Model, an adaptive learning rate value can be achieved by an updating mechanism using the $0 < \mu(t)Y_m(\rho) < 2\dot{\eta}(t)$ criteria instead of a fixed learning value. An adaptive learning rate value bounded by $2\dot{\eta}(t)$ value to ensure convergence and stability of ROV and USV platforms are presented in Fig. 10 and Fig. 11.

Based on the stability and robustness of the converged system for the ROV and USV platforms, it required that the optimal learning rate value fulfils the $0 < \mu(t)\dot{Y}_M(t) < 2\dot{\eta}(t)$ boundary condition. By selecting or adjusting a proper learning rate value, the feedback control structure will be stable and ensure the convergence process. In order to improve the convergence speed and stability, an adaptive learning rate is applied which is a value updated on each iteration by selecting a maximum boundary of the learning rate value to 90 % of the $2\dot{\eta}(t)$ value. This will ensure the stability and robustness of the feedback system. The proper value of the learning rate not only provides stability and robustness of the nonlinear system but also improves the convergence speed process and produces a smaller MSE value. The coupled U-Model adaptive learning rate approach can be useful for an unknown nonlinear system to reduce the time duration of the tuning process. Most of the control synthesis requires to be tuned appropriately at an early stage for the system to converge on to the desired reference value. The adaptive learning rate approach not only ensures a faster convergence time but also ensures the learning process of the model is in the stable region. The results for the proposed approach are promising for real-time implementation, where the computational complexity is of major concern. The U-model based approach provides a simple control law synthesis that can be compared to more accurate but complex techniques such as the multi-loop adaptive control approach [24].

VI. CONCLUSION

The findings of the simulations demonstrate that adaptive coupled underactuated multivariable nonlinear control strategies can be implemented for the UMV platform with parameter uncertainties. The coupled U-Model approach only requires a suitable initial condition range from 0 to 1 for all the parameters, weights, and appropriate learning rate values

for better stability and convergence speed. The U-model IMC incorporated with the forward propagation of RBF neural networks approach includes adaptive and learning capabilities to reduce the error between the model and the multivariable nonlinear UMV system for better control synthesis to sustain the stability of the system. RBF neural networks capable to approximates the nonlinearity as universal approximator with only one-layer network for faster computation. U-Model IMC provides a good solution in control inverse formulation due to nonlinear modelling approach is a polynomial equation thus the inverse equation exists and feasible to compute. U-Model IMC scheme provides better control performance and disturbance rejection capability as demonstrate in USV platform simulation by introducing external sway speed towards the platform. This nonlinear control approach can minimise the time duration of the controller design by implementing an adaptive learning rate method for the unknown control system. This nonlinear controller will be implemented in the real-time experiment using open source Robot Operating System (ROS) architecture on GIRONA 500 UUV platform at Girona Underwater Vision and Robotics for future work.

REFERENCES

[1] G. A. Demetriou, A. Hadjipieri, I. E. Panayidou, A. Papasavva, and S. Ioannou, "ERON: A PID controlled autonomous surface vessel," in *Proc. 18th Medit. Electrotech. Conf. (MELECON)*, Apr. 2016, pp. 1–5.

[2] C. Shen, B. Buckham, and Y. Shi, "Modified C/GMRES algorithm for fast nonlinear model predictive tracking control of AUVs," *IEEE Trans. Control Syst. Tech.*, vol. 25, no. 5, pp. 1896–1904, Sep. 2017.

[3] A. Manzanilla, P. Castillo, and R. Lozano, "Nonlinear algorithm with adaptive properties to stabilize an underwater vehicle: Real-time experiments," *IFAC-PapersOnLine*, vol. 50, no. 1, pp. 6857–6862, 2017.

[4] Y. Shen, K. Shao, W. Ren, and Y. Liu, "Diving control of autonomous underwater vehicle based on improved active disturbance rejection control approach," *Neurocomputing*, vol. 173, pp. 1377–1385, Jan. 2016.

[5] D. L. Rudnick, R. E. Davis, C. C. Eriksen, D. M. Fratantoni, and M. J. Perry, "Underwater gliders for ocean research," *Marine Technol. Soc. J.*, vol. 38, no. 2, pp. 73–84, 2004.

[6] Y. Wang, S. Jiang, B. Chen, and H. Wu, "Trajectory tracking control of underwater vehicle-manipulator system using discrete time delay estimation," *IEEE Access*, vol. 5, pp. 7435–7443, Jun. 2017.

[7] Unmanned Surface Vessels Under Development. (2014). *Maritime Journal Insight for the European Commercial Business*. Accessed: Aug. 21, 2019. [Online]. Available: https://www.maritimejournal.com/news101/marine-civils/hydrographic-survey/unmanned-surface-vessels-under-development

[8] Forum Energy Technologies. (2019). *XLX 200HP Work Class ROV*. [Online]. Available: https://www.f-e-t.com/products/drilling-and-subsea/subsea-technologies/rovs/rovs-work-class/triton-xls-heavy-duty-work-class-rov.

[9] (2017). *General Dynamics Announces Availability of Bluefin SandShark AUV*. Accessed: Aug. 19, 2019. [Online]. Available: https://www.unmannedsystemstechnology.com/2017/01/general-dynamics-announces-availability-bluefin-sandshark-auv/

[10] UW News School of Oceanography College of the Environment. (2013). *Seaglider Licensed to Kongsberg*. [Online]. Available: https://www.ocean.washington.edu/story/Seaglider_Licensed_to_Kongsberg

[11] Z. Zheng, L. Ruan, and M. Zhu, "Output-constrained tracking control of an underactuated autonomous underwater vehicle with uncertainties," *Ocean Eng.*, vol. 175, pp. 241–250, Dec. 2019.

[12] J. Guerrero, J. Torres, V. Creuze, and A. Chemori, "Trajectory tracking for autonomous underwater vehicle: An adaptive approach," *Ocean Eng.*, vol. 172, pp. 511–522, Dec. 2019.

[13] B. Huang and Q. Yang, "Double-loop sliding mode controller with a novel switching term for the trajectory tracking of work-class ROVs," *Ocean Eng.*, vol. 178, pp. 80–94, Aug. 2019.

[14] I. L. G. Borlaug, K. Y. Pettersen, and J. T. Gravdahl, "Trajectory tracking for an articulated intervention AUV using a super-twisting algorithm in 6 DOF?" *IFAC-PapersOnLine*, vol. 51, no. 29, pp. 311–316, 2018.

[15] J. Guerrero, E. Antonio, A. Manzanilla, J. Torres, and R. Lozano, "Autonomous underwater vehicle robust path tracking: Auto-adjustable gain high order sliding mode controller," *IFAC-PapersOnLine*, vol. 51, no. 13, pp. 161–166, 2018.

[16] Y. Wang, K. Zhu, B. Chen, and M. Jin, "Model-free continuous nonsingular fast terminal sliding mode control for cable-driven manipulators," *ISA Trans.*, to be published.

[17] Y. Wang, L. Liu, D. Wang, F. Ju, and B. Chen, "Time-delay control using a novel nonlinear adaptive law for accurate trajectory tracking of cable-driven robots," *IEEE Trans. Ind. Informat.*, to be published.

[18] A. Balasuriya and L. Li Cong, "Adaptive fuzzy sliding mode controller for underwater vehicles," in *Proc. 4th Int. Conf. Control Automat. (ICCA)*, 2003, pp. 917–921.

[19] C. P. Bechlioulis, G. C. Karras, S. Heshmati-Alamdari, and K. J. Kyriakopoulos, "Trajectory tracking with prescribed performance for underactuated underwater vehicles under model uncertainties and external disturbances," *IEEE Trans. Control Syst. Technol.*, vol. 25, no. 2, pp. 429–440, Mar. 2016.

[20] C. Lv, "A hybrid coordination controller for speed and heading control of underactuated unmanned surface vehicles system," *Ocean Eng.*, vol. 176, pp. 222–230, Mar. 2019.

[21] H. Huang, M. Gong, Y. Zhuang, S. Sharma, and D. Xu, "A new guidance law for trajectory tracking of an underactuated unmanned surface vehicle with parameter perturbations," *Ocean Eng.*, vol. 175, pp. 217–222, Aug. 2019.

[22] G. Zhang and X. Zhang, "Concise robust adaptive path-following control of underactuated ships using DSC and MLP," *IEEE J. Ocean. Eng.*, vol. 39, no. 4, pp. 685–694, Oct. 2014.

[23] W. Caharija, K. Y. Pettersen, M. Bibuli, P. Calado, E. Zereik, J. Braga, J. T. Gravdahl, A. J. Sørensen, M. Milovanovic, and G. Bruzzone, "Integral line-of-sight guidance and control of underactuated marine vehicles: Theory, simulations, and experiments," *IEEE Trans. Control Syst. Technol.*, vol. 24, no. 5, pp. 1623–1642, Sep. 2016.

[24] M. Medvedev and V. Pshikhopov, "Multi-loop adaptive control of mobile object path," in *Proc. 12th Asian Control Conf. (ASCC)*, 2019, vol. 444, no. 1, pp. 444–449.

[25] Y. Bouzid, H. Siguerdidjane, and Y. Bestaoui, "Nonlinear internal model control applied to VTOL multi-rotors UAV," *Mechatronics*, vol. 47, pp. 49–66, Nov. 2017.

[26] J. Singh, K. Chattterjee, and C. B. Vishwakarma, "Two degree of freedom internal model control-PID design for LFC of power systems via logarithmic approximations," *ISA Trans.*, vol. 72, pp. 185–196, Jan. 2018.

[27] Q. M. Zhu and L. Z. Guo, "A pole placement controller for non-linear dynamic plants," *Proc. Inst. Mech. Eng., I, J. Syst. Control Eng.*, vol. 216, no. 6, pp. 467–476, Sep. 2002.

[28] T. Khan and M. Shafiq, "A novel internal model control scheme for adaptive tracking of nonlinear dynamic plants," in *Proc. 1st IEEE Conf. Ind. Electron. Appl.*, no. 1, May 2006, pp. 1–6.

[29] M. Shafiq and T. Khan, "Newton-Raphson based adaptive inverse control scheme for tracking of nonlinear dynamic plants," in *Proc. 1st Int. Symp. Syst. Control Aerosp. Astronaut. (ISSCAA)*, Jan. 2006, p. 1343.

[30] Q. M. Zhu and Z. Ma, "A U-model enhanced PID controller for nonlinear dynamic plants," in *Proc. 6th World Congr. Intell. Control Automat. (WCICA)*, vol. 1, 2006, pp. 1026–1029.

[31] S. S. A. Ali, F. M. Al-Sunni, M. Shafiq, and J. M. Bakhashwain, "U-model based learning feedforward control of MIMO nonlinear systems," *Elect. Eng.*, vol. 91, no. 8, pp. 405–415, 2010.

[32] I. Abbasi, S. S. A. Ali, R. Ibrahim, S. H. Adil, and M. Ovinis, "U-model based depth control of underwater glider," in *Proc. Int. Conf. Inf. Commun. Technol. (ICICT)*, 2015, pp. 1–4.

[33] Z. Chu, D. Zhu, and S. X. Yang, "Observer-based adaptive neural network trajectory tracking control for remotely operated vehicle," *IEEE Trans. Neural Netw. Learn. Syst.*, vol. 28, no. 7, pp. 1633–1645, Jul. 2017.

[34] I. Abbasi, S. S. A. Ali, M. Ovinis, and W. Naeem, "U-model based controller design for an unmanned free swimming submersible (UFSS) vehicle under hydrodynamic disturbances," *Indian J. Geo-Mar. Sci.*, vol. 46, no. 4, pp. 742–748, 2017.

[35] N. A. A. Hussain, S. S. A. Ali, M. N. M. Saad, and M. Ovinis, "Underactuated nonlinear adaptive control approach using U-model for multivariable underwater glider control parameters," in *Proc. IEEE 6th Int. Conf. Underwater Syst. Technol., Theory Appl.*, Dec. 2016, pp. 19–25.

[36] S. S. A. Ali, M. Moinuddin, K. Raza, and S. H. Adil, "An adaptive learning rate for RBFNN using time-domain feedback analysis," *Sci. World J.*, vol. 2014, Mar. 2014, Art. no. 850189.
[37] M. Shafiq and N. R. Butt, "U-model based adaptive IMC for nonlinear dynamic plants," in *Proc. 10th IEEE Conf. Emerg. Technol. Factory Automat. (ETFA)*, vol. 1, Sep. 2005, p. 959.
[38] R. Rout, B. Subudhi, and S. Mahapatra, "Development of a NARMAX based constraint-adaptive heading controller for an autonomous underwater vehicle," in *Proc. OCEANS*, 2016, pp. 1–5.
[39] D. Lam and D. Wunsch, "Unsupervised feature learning classification with radial basis function extreme learning machine using graphic processors," *IEEE Trans. Cybern.*, vol. 47, no. 1, pp. 224–231, Jan. 2017.
[40] R. U. Amin, L. Aijun, L. Hongshi, and L. Jiaxing, "An adaptive sliding mode control based on radial basis function network for attitude tracking control of four rotor hover system," in *Proc. IEEE Chin. Guid., Navigat. Control Conf. (CGNCC)*, Aug. 2016, pp. 580–585.
[41] T. Mutaz and A. Ahmad, "Solar radiation prediction using radial basis function models," in *Proc. Int. Conf. Develop. E-Syst. Eng. (DeSE)*, 2015, pp. 77–82.
[42] S. S. A. Ali, "U-model based multivariable nonlinear adaptive control," Ph.D. dissertation, Dept. Elect. Syst. Eng., King Fahd Univ. Petroleum Minerals, Dhahran, Saudi Arabia, 2007.
[43] A. Syed, S. Azhar, F. M. Al-Sunni, M. Shafiq, J. M. Bakhashwain, and S. S. Azhar, "MIMO U-model based control?: Real-time tracking control and feedback analysis via small gain theorem," *WSEAS Trans. Circuits Syst.*, vol. 7, no. 7, pp. 610–619, 2008.
[44] M. Rupp and A. H. Sayed, "A time-domain feedback analysis of filtered-error adaptive gradient algorithms," *IEEE Trans. Signal Process.*, vol. 44, no. 6, pp. 1428–1439, Jun. 1996.
[45] B. Hassibi, A. H. Sayed, and T. Kailath, "H^∞ optimality of the LMS algorithm," *IEEE Trans. Signal Process.*, vol. 44, no. 2, pp. 267–280, Feb. 1996.
[46] C. S. Chin, *Computer-Aided Control System Design: Practical Application Using MATLAB and Simulink*. New York, NY, USA: Taylor & Francis, 2013.
[47] T. I. Fossen, *Marine Control System Guidance, Navigation and Control of Ships, Rigs and Underwater Vehicles*, 2nd ed. Trondheim, Norway: Marine Cybernetics, 2002.
[48] F. J. Velasco, E. R. Herrero, E. López, and E. Moyano, "Identification for a heading autopilot of an autonomous in-scale fast ferry," *IEEE J. Ocean. Eng.*, vol. 38, no. 2, pp. 263–274, Apr. 2013.
[49] K. S. M. Davidson and L. Schiff, "Turning and course keeping qualities," *Trans. Soc. Nav. Archit. Mar. Eng.*, vol. 54, 1946.
[50] M. S. M. Aras, S. S. Abdullah, A. A. Rahman, and M. A. A. Aziz, "Thruster modelling for underwater vehicle using system identification method," *Int. J. Adv. Robot. Syst.*, vol. 10, no. 5, p. 252, Jan. 2013.

NUR AFANDE ALI HUSSAIN received the Bachelor of Engineering (Electrical) degree (Hons.) from Universiti Teknologi Malaysia (UTM), in 2003, and the M.Sc. degree in electrical and electronic engineering from Universiti Sains Malaysia (USM), in 2014. He is currently pursuing the Ph.D. degree in electrical and electronic engineering with Universiti Teknologi PETRONAS (UTP), Malaysia, in Adaptive non-linear MIMO control system for marine robotics. His research interest is in unmanned control system engineering and a former Visiting Researcher at Girona Underwater Vision and the Robotics University of Girona Spain.

SYED SAAD AZHAR ALI received the B.S. degree from the NED University of Engineering and Technology, Pakistan, in 1999, and the M.S. and Ph.D. degrees in electrical engineering from the King Fahd University of Petroleum and Minerals, in 2001 and 2007, respectively. He joined the King Fahd University of Petroleum and Minerals, Saudi Arabia, in 2000. He served Air University and Iqra University, Pakistan, prior to joining the Center for Intelligent Signal and Imaging Research, Universiti Teknologi PETRONAS (UTP), Malaysia, as an Associate Professor with areas of research in nonlinear control and signal processing.

MARK OVINIS received the Bachelor of Mechanical Engineering degree (Hons.) from Universiti Teknologi Malaysia (UTM), in 1999, the M.Eng. degree in mechanical engineering from Texas A&M, USA, in 2003, and the Ph.D. degree from Loughborough University, U.K., in 2011. He is currently a Senior Lecturer with the Mechanical Engineering Department, Universiti Teknologi PETRONAS (UTP). His research interest is in underwater robotics.

MOHD RIZAL ARSHAD received the B.Eng. degree in medical electronics and instrumentation from the University of Liverpool, U.K., in July 1994, the M.Sc. degree in electronic control engineering from the University of Salford, in 1995, and the Ph.D. degree in electrical engineering from the University of Liverpool, in 1999. He is currently a Full Professor with Universiti Sains Malaysia Engineering Campus, Nibong Tebal, Malaysia. His areas of specialization are ocean robotics and instrumentation, control, and intelligent system for industrial applications.

UBAID M. AL-SAGGAF received the B.Sc. degree (Hons.) in electrical engineering and the B.Sc. degree (Hons.) in mathematics from the King Fahd University of Petroleum and Minerals, Dhahran, Saudi Arabia, in 1980, and the M.Sc. and Ph.D. degrees in electrical engineering from Stanford University, Stanford, USA, in 1983 and 1986, respectively. He was appointed as an Assistant Professor with the King Fahd University of Petroleum and Minerals, in 1986 and then an Associate Professor in 1991. He was on leave from 1992 to 2010 and worked for the Ministry of Defence and Aviation as an Executive Technical Advisor for the Research and Development Department. He joined the Electrical and Computer Engineering Department, King Abdulaziz University, in 2010, where he is currently a Professor. He is also the Director of the Center of Excellence in Intelligent Engineering Systems (CEIES), King Abdulaziz University, and the Director of Innovation and Prototyping Center (IPC), King Abdulaziz University.